Effect of microelectrode array spacing on the growth of platinum electrodeposits and its implications for oxygen sensing in ionic liquids

Junqiao Lee, Jesse Mullen, Ghulam Hussain, Debbie S. Silvester*

School of Molecular and Life Sciences, Curtin University, GPO Box U1987, Perth, WA 6845, Australia.

*E-mail: d.silvester-dean@curtin.edu.au; Tel: +61(8)92667148

For the virtual special issue: ISE Belgrade Online meeting: Symposium 2

Abstract

Microelectrodes are popular in electroanalysis because radial diffusion to the electrodes results in high current density. The current can then be multiplied by increasing the number of electrodes in an array configuration, allowing for low concentrations of analyte species to be detected. Microelectrode arrays are usually designed so that individual microelectrodes (in a hexagonal arrangement) are sufficiently spaced, ensuring that diffusion layers do not overlap during electrochemical experiments, but are not too far separated so that space is wasted. In this study, the effect of microelectrode spacing has been investigated for platinum deposition into the microholes of commercially available microarray devices. The microarrays have 91 recessed microelectrodes, 10 μm in diameter, 3.3 μm depth, but with four different centre-to-centre spacings of 80, 60, 40 and 20 μm (8, 6, 4 and 2 times the diameter). A 300 second deposition time in an aqueous hexachloroplatanic acid solution was used to deposit three-dimensional Pt structures into the array. The size of the deposits systematically decreased as the electrode spacing became smaller, as a result of overlapped diffusion layers during the deposition process. The modified microarrays were then used for the sensing of a model analyte (oxygen) in a room temperature ionic liquid, with the larger deposits (with larger surface areas) giving higher current responses. However, current densities were found to be quite comparable for all spacings. The 2 times diameter separation can theoretically fit 16 times the number of electrodes into the same area of the underlying Au electrode compared to the 8 times separation. Therefore, it should be possible to design devices that have significantly higher electrode density, which can maximise the overall current and lead to better analytical performances. This work shows that it is important to consider both the geometry and electrode separation for microarrays when used in electrodeposition and for electroanalytical applications.

Keywords

Microelectrode arrays; electrodeposition; overlapping diffusion; platinum deposition; oxygen sensing; room temperature ionic liquids.

1. Introduction

Electrochemistry is becoming increasingly important in different applications, including batteries, fuel cells, supercapacitors and sensors.[1, 2] The role of the electrode material and its geometry is vital for many of these applications, and optimising the electrode material and design is often the focus for many researchers. Over the last several years, low-cost planar electrode devices, such as screen-printed electrodes (SPEs),[3-8] thin-film electrodes (TFEs)[9-17] and microarray thin-film electrodes[18-21] have become increasingly available to researchers, and used for electroanalysis. Their simple design makes for facile miniaturisation, as well as significantly reducing the overall amount of electrode materials and assembly cost.

For electrochemical sensing applications, the use of microelectrodes – which have at least one dimension smaller than 100 µm and typically 10–50 µm [22] – leads to vastly different diffusional properties compared to larger macroelectrodes. Higher current densities and greater sensitivities are possible because of the enhancement of mass transport (radial diffusion) at microelectrodes compared to macroelectrodes (predominantly linear diffusion). Because the overall current at a microelectrode is lower (owing the small electrode area), the current can be further enhanced by employing multiple electrodes in an "array" configuration.[22] The electrochemical behaviour of regularly spaced microelectrode arrays has been described by various researchers using both experiment and theory,[11, 23-26] and some have also discussed in detail the impact of overlapping diffusion profiles during electroanalysis.[27] Davies and Compton[23] performed extensive digital simulation, followed up by experimental studies,[24] to show the impact of overlapping diffusion layers on inlaid disk electrodes. Although there have been various different recommendations,[28-30] the generally accepted electrode spacing is ten times the diameter, with the electrodes in a hexagonal arrangement to minimise diffusion zone overlap; this the standard design available from most electrode manufacturers.

Microelectrode arrays are available commercially in planar devices, with the working electrode (WE) integrated with a counter and reference electrode. However, to keep the costs low in the manufacturing process, the WE design is usually limited to recessed electrodes, where an underlying metal electrode surface is covered with an inert polymer layer (e.g. SU-8) and multiple holes in the layer expose an array of recessed microdisk electrodes. One way to enhance the sensitivity of these recessed microelectrodes is to modify the arrays by electrodeposition to fill the holes and create three-dimensional structures.[20] Electrodeposition is a well-established electrochemical technique that can produce electrode surfaces with enhanced electrocatalytic properties using only small quantities of electrocatalysts.[31-33] Using chronoamperometry or voltammetry, the potential is typically stepped/scanned to the reduction potential of the electrocatalyst to deposit the reduced species onto the working electrode surface. Platinum is a well-known electrocatalyst[31, 32] for the reduction of oxygen, as well as for the oxidation of ammonia and hydrogen. The electrodeposition of platinum is often performed in aqueous solutions of hexachloroplatinic acid (H_2PtCl_6). The metal complex is reduced to metallic platinum according to equations 1 and 2:[31]

$$PtCl_6^{2-}{}_{(aq)} + 2e^- \rightleftharpoons PtCl_4^{2-}{}_{(aq)} + 2Cl^-{}_{(aq)} \quad (1)$$

$$PtCl_4^{2-}{}_{(aq)} + 2e^- \rightleftharpoons Pt_{(s)} + 4Cl^-{}_{(aq)} \quad (2)$$

We have previously demonstrated the electrodeposition of platinum into commercially available recessed microelectrode arrays with ten times the diameter separation, forming three-dimensional cauliflower-shaped segmented nanostructures.[20, 21] Remarkable improvements in the sensitivity (up to 16-fold) towards both oxygen and ammonia in room temperature ionic liquids (RTILs) were achieved, but this was significantly lower than the 44 times increase in electroactive surface area (ESA) from the deposits. This is likely due to overlapping diffusion layers established by the newly-protruding conductive surfaces.[20, 34]

In this work, we investigate the impact of electrode spacing on the metal electrodeposition process for the first time. The electrodes are regularly spaced in a hexagonal arrangement with centre-to-centre distances of 8 times, 6 times, 4 times and 2 times the diameter of an individual microhole. It is expected that there will be significant diffusion layer overlap at the very closely spaced electrode (see Figure 1, top) compared to the more widely spaced electrodes that should have individual diffusion layers (see Figure 1, bottom) especially at short timescales. The plating bath solution and deposition conditions are kept constant so that the deposition process is only affected by the microelectrode spacing. The modified electrodes are then utilised as sensing devices to detect oxygen gas as a model analyte in a RTIL, to compare the analytical performance, which will inform the most optimal modified-electrode design for sensing. We note that the impact of electrode spacing on metal electrodeposition over non-inlaid (recessed or protruding) surfaces has not yet been studied.

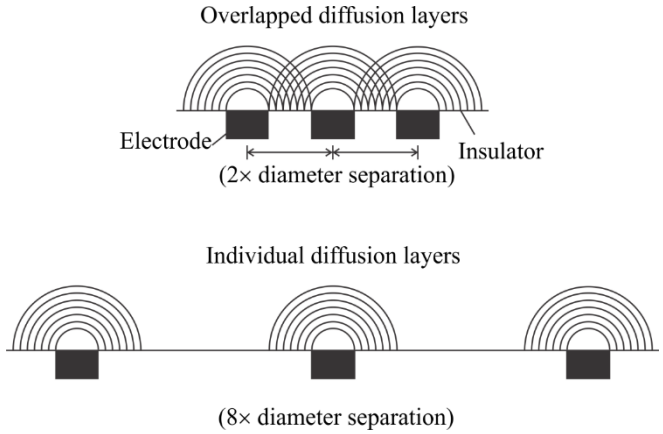

Figure 1: Schematic diagram of diffusion profiles of inlaid microarrays with adjacent electrodes placed very close together (2 times the diameter spacing), and electrodes that are sufficiently separated (8 times the diameter separation). In the case of closely-packed electrodes, the diffusion layers overlap significantly such that planar (linear) diffusion rapidly dominates for the electrodes in the centre of the array.

2. Experimental

2.1 Chemicals and Reagents

Hexachloroplatinic acid hydrate ($H_2PtCl_6.6H_2O$, trace metal basis, ≥ 99.9%, Sigma-Aldrich, Castle Hill, NSW, Australia), hexaammineruthenium (III) chloride ($[Ru(NH_3)_6]Cl_3$, 98%, Merck, Kilsyth, VIC, Australia), potassium nitrate (KNO_3, >99.5 %, Chem-Supply, Gillman, SA, Australia), acetone (99%, Sigma-Aldrich, Castle Hill, NSW, Australia) and sulfuric acid (H_2SO_4, 98% w/w, Merck, Kilsyth, VIC, Australia) were used as received. The room temperature ionic liquid (RTIL) *N*-butyl-*N*-methylpyrrolidinium bis(trifluoromethylsulfonyl)imide ($[C_4mpyrr][NTf_2]$, >99.5 %) was purchased from Merck (Kilsyth, VIC, Australia), at ultra-high purity electrochemical grade, and used as received. Ultrapure water with a resistance of 18.2 MΩ cm was prepared by an ultrapure water purification system (Millipore Pty Ltd., North Ryde, NSW, Australia). Oxygen (O_2) and nitrogen (N_2) gases at 99.99 % were purchased from Coregas Pty. Ltd. (Jandakot, WA, Australia).

2.2 Electrochemical experiments

All experiments were performed using a PGSTAT101 Autolab potentiostat (Metrohm Autolab, Netherlands) interfaced to a PC with Nova 1.11 software, at laboratory room temperature (294±1 K) inside an aluminium Faraday cage to reduce electrical interference. Custom-made gold microarray thin-film electrodes (MATFEs, Micrux Technologies, Oviedo, Spain) were used throughout this study, consisting of a 1 mm diameter disk shaped Au thin-film (150 nm) deposited on a Pyrex glass substrate. A layer of SU-8 polymer is used to define the arrays, which consist of 91 µ-holes of 10 µm in diameter in a hexagonal arrangement. All of the electrodes were fabricated on a single glass substrate to ensure the same height of the casted SU-8 layer (see section 2.5). The centre-to-centre distance between the µ-holes was varied between devices: 80 µm (8× diameter), 60 µm (6× diameter), 40 µm (4× diameter) and 20 µm (2× diameter) using a custom-made template from the manufacturer. The MATFEs contain inbuilt Au thin-film counter and quasi-reference electrodes.

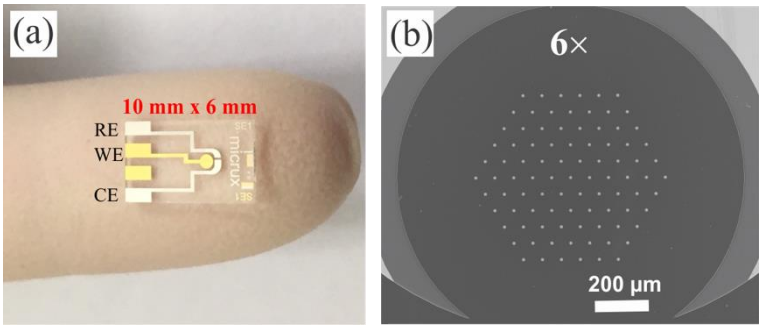

Figure 2: (a) Photo of a TFE, showing the connecting pads that attach to the reference electrode (RE), working electrode (WE) and counter electrode (CE). (b) SEM image of the working electrode surface of an unmodified array with 6× centre-to-centre spacing on an underlying gold electrode (diameter 1 mm). The MATFE contains 91 recessed microelectrodes with a diameter of 10 µm, confined within an SU-8 polymer layer of height 3.25 µm.

All MATFEs were thoroughly washed with acetone and water to remove any residue from the manufacturing process. They were then electrochemically activated in 0.5 M $H_2SO_{4\ (aq)}$ by scanning the potential between -0.40 and +1.80 V vs an external Ag/AgCl (0.1 M KCl) reference electrode (BASi, Indiana, USA) and a Pt coil

counter electrode at a sweep rate of 1 V s^{-1} for ca. 300 cycles. The electrodes were then washed with ultrapure water and dried under a flowing stream of nitrogen.

The MATFEs were modified by electrodeposition of Pt into the recessed µ-holes using a plating bath containing 20 mM H_2PtCl_6 in 0.5 M H_2SO_4. Prior to deposition, two cyclic voltammograms at a scan rate of 1 V s^{-1} were first recorded to check that the deposition potential was as expected, and stable with repeat scans. The potential was then stepped from the open circuit potential (OCP, ~+0.70 V) to -0.2 V (vs an external Ag/AgCl) and held for 300 seconds,[20] which was found to be optimum to produce the desired structures in this work. The rate of mass transport was fixed by using a magnetic stirrer at 650 rpm and the positions and orientations of the MATFE and external counter electrode were kept as constant as possible for all experiments. We had previously optimised the electrodeposition parameters (stirring/no stirring, deposition time, concentration, potential) for the 10× separation.[20] These parameters have been kept constant in this work to focus only on the effect of electrode separation.

2.3 Oxygen gas sensing experiments

For O_2 gas sensing experiments, the electrodes were placed into the slit of a modified rubber stopper and inserted into a home-made glass cell. 2 µL of RTIL was drop-cast on the TFE to cover all three electrodes. Prior to the introduction of oxygen, the cell was purged with nitrogen (N_2) gas for at least one hour to remove dissolved impurities. To achieve different concentrations, O_2 gas was diluted with N_2 gas using two digital flow meters (0–1.0 L min^{-1}, John Morris Scientific, Sydney, NSW, Australia) – one connected to the O_2 cylinder and the other the N_2 cylinder through PTFE tubing – via a Swagelok T-joint (Swagelok, Kardinya, WA, Australia) as reported in detail in the supplementary information of Lee et al.[9] The concentration of O_2 gas introduced into the T-cell was calculated using the relative flow rates of the two gases.

2.4 Electrode imaging

Scanning electron microscopy (SEM) images were taken using a Neon (Zeiss Neon 40 EsB FIB-SEM), with an accelerating voltage of 5.0 kV, a working distance of ca. 7 mm, and an aperture size of 30 µm, using an in-lens detector. Prior to imaging, all modified MATFEs were first visually inspected using optical microscopy to confirm that uniform deposition occurred across the microarrays and that all microholes were filled. The samples were coated with a ~3 nm layer of platinum for SEM imaging to minimise the charging current due to the presence of the insulating SU-8 layer.

2.5 Thickness measurements

Atomic force microscopy was used to measure the thickness of the SU-8 layer using an atomic force microscope (Bruker Dimension Icon AFM; Hilton, Adelaide, Australia). Three electrode devices for each of the four electrode separations were measured, and a thickness of 3.28 (±0.03) µm was measured, which was highly consistent over all devices. The height of the Pt deposits above the SU-8 layer were measured using a confocal microscope (WITec alpha300 series, Ulm, Germany) with 100 × magnification lenses. This was carried out by manually focusing at the base (top of SU-8 film) and refocussing at the top of the deposited platinum structures.

More than 10 different deposits were measured for each MATFE spacing. The heights were averaged, and one standard deviation was calculated as the uncertainty.

3. Results and Discussion

The effect of electrode separation on the growth of platinum electrodeposits was investigated for hexagonally arranged microelectrode arrays with four different center-to-center separations of 8, 6, 4 and 2 times the diameter of a single microdisk (referred to in this paper as 8×, 6×, 4×, and 2× spacing). The number of electrodes in each device was kept constant (91) over the whole electrode, so that the behaviour is dependent only on the spacings between the electrodes. The microarrays were fabricated onto a single wafer to ensure that the microhole recession depth (defined by the thickness of the SU-8 layer) was consistent for all spacings. The electrodeposited structures and their growth mechanisms can be compared with that described previously by our group under similar conditions on standard (10×) commercially available MicruX Pt MATFEs.[20]

3.1 Electrodeposition of 3D Pt structures from H_2PtCl_6 plating bath

Figure 3 shows typical chronoamperometric transients for the deposition of platinum (from a 20 mM $H_2PtCl_6.6H_2O$/0.5 M H_2SO_4 plating bath) into the microholes of the different Au electrode designs (8×, 6×, 4× and 2×) employed in this work. The potential was held at -0.2 V vs an external Ag/AgCl reference electrode for 300 seconds and the current was monitored as a function of time. After the initial seeding period, the magnitude of the current increases consistently during the growth process due to the gradual increase in electroactive surface area. At short times (t < 50 seconds) – representing initial filling of the microholes – the transient is fairly consistent for all electrode separations (Figure 3). This is likely caused by the recessed electrode design, where linear diffusion is expected to dominate due to the confinement of mass transport within the microholes. At longer times, larger deviations in the overall currents (and total charge) are observed as a result of significant diffusion layer overlap occurring during the deposition process, especially for the more closely spaced electrodes. Oscillations in the current are thought to be caused by the formation of rough platinum growths over the edge of the microhole,[21] which get increasingly larger as the deposition progresses.

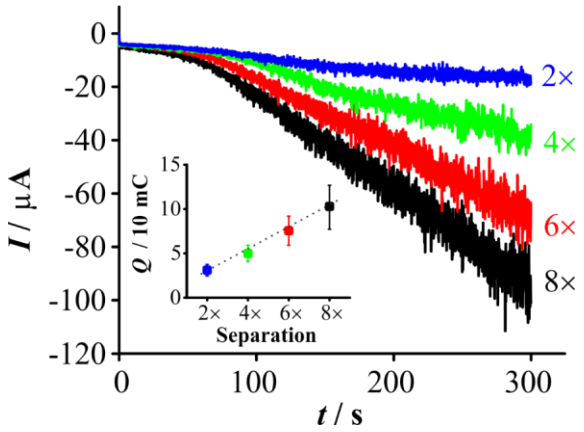

Figure 3: Chronoamperometric transients for the deposition of Pt (from 20 mM $H_2PtCl_6.6H_2O$ in 0.5 M H_2SO_4, –0.2 V vs Ag/AgCl) on Au MATFEs with different centre-to-centre spacing, labelled as 8×, 6×, 4× and 2×, relative to the diameter of an individual microelectrode (10 μm). The inset shows the charge (Q) under the deposition curve, with error bars representing one standard deviation of four repeat depositions on different Au MATFEs.

To estimate the amount of material deposited, the charge (Q) under the deposition curve was calculated from the integrated area ($Q = \int I \, dt$), where I is the current (A) and t is the time (s). A plot of average deposition charge as a function of electrode separation is shown in the inset to Figure 3. Consistent with overlapped diffusion layers during the deposition, the charge is the lowest for the most closely packed electrodes (2x), and highest for the most widely separated electrodes (8x), despite using the same concentration of plating bath solution and the same deposition time. A slightly larger variation in deposition charge is observed for the more widely separated electrodes, as indicated by the increased error bars. Scanning electron microscopy (SEM) images of the whole electrode with the deposits are shown in Figure 4 for all four electrode separations. All holes appear to be consistently filled across the array, with every hole overfilled with a physically stable three-dimensional Pt structure, as was observed previously for the 10x separation.[20]

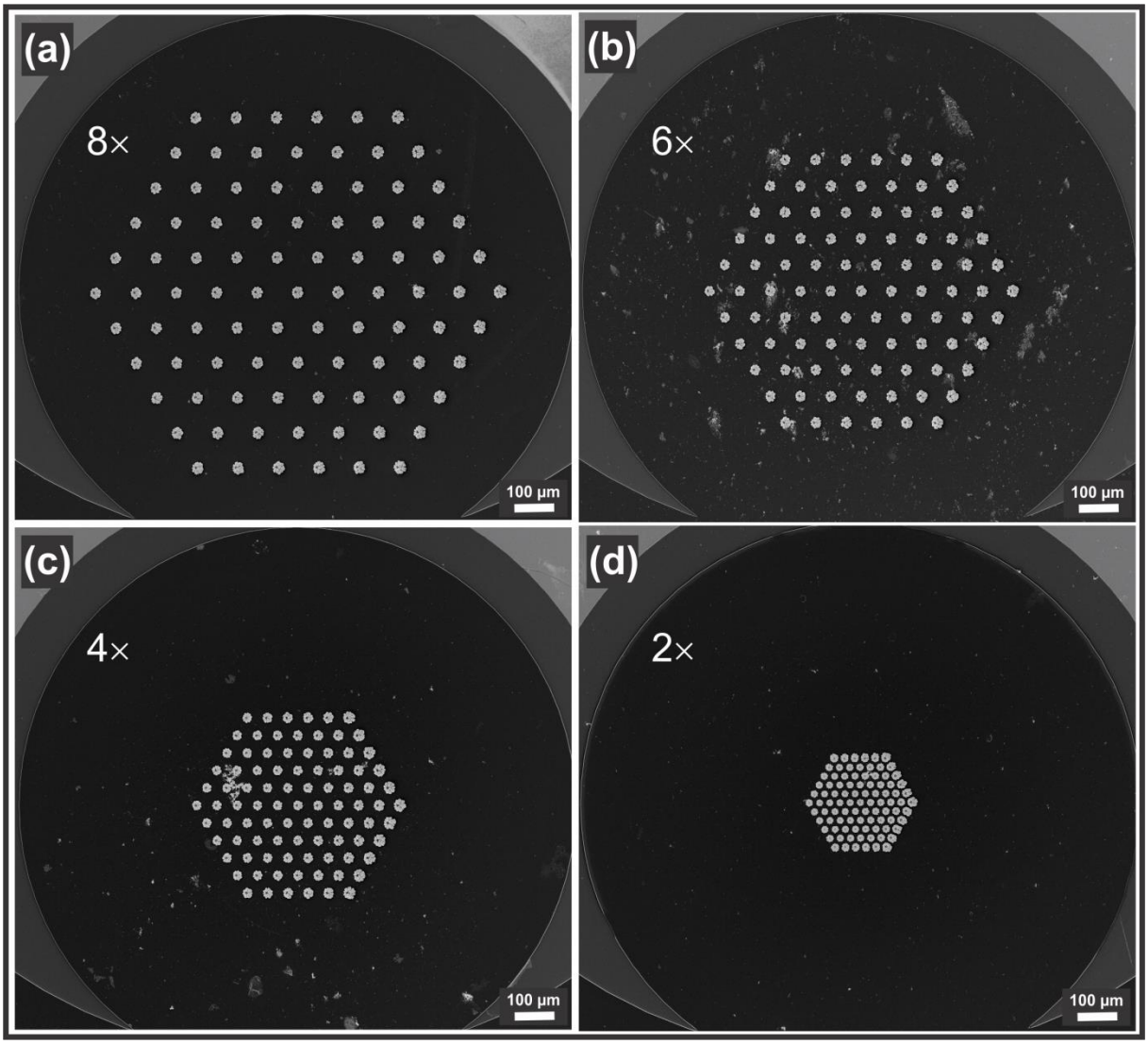

Figure 4: Scanning electron microscopy (SEM) images of working electrodes formed after the deposition of 3D platinum structures into Au recessed MATFEs. Four different centre-to-centre spacings are shown: (a) 8x, (b) 6x, (c) 4x, and (d) 2x the diameter.

Figure 5 shows close-up images of seven electrodes within the arrays, showing similar shapes, but with slight variations between the different deposits within the array. Even further close-up images of a single microhole with a Pt deposit are shown in Figure S1 in the supporting information. The 'cauliflower' type shape is similar

to our previous report,[20] with a hole in the centre of the deposit caused by linear diffusion within the microhole, and enhanced deposits around the hole due to increased radial diffusion at the edges. We note that the underlying electrode surface is gold in this study, compared to platinum in the previous study, which may change the deposition amount and its morphology slightly. The images in Figure 5 show an increased amount of deposit to one side of the microholes (right side of the image), which is likely caused by higher flux to one side of the electrode as a result of stirring the solution during the deposition process. This was consistent on several repeated depositions on the underlying gold electrode surface. This is less noticeable for the 2x separation for the electrode in the centre of the array (Figure 5d), but still very obvious for the electrodes at the edge of the array (see Figure 4d).

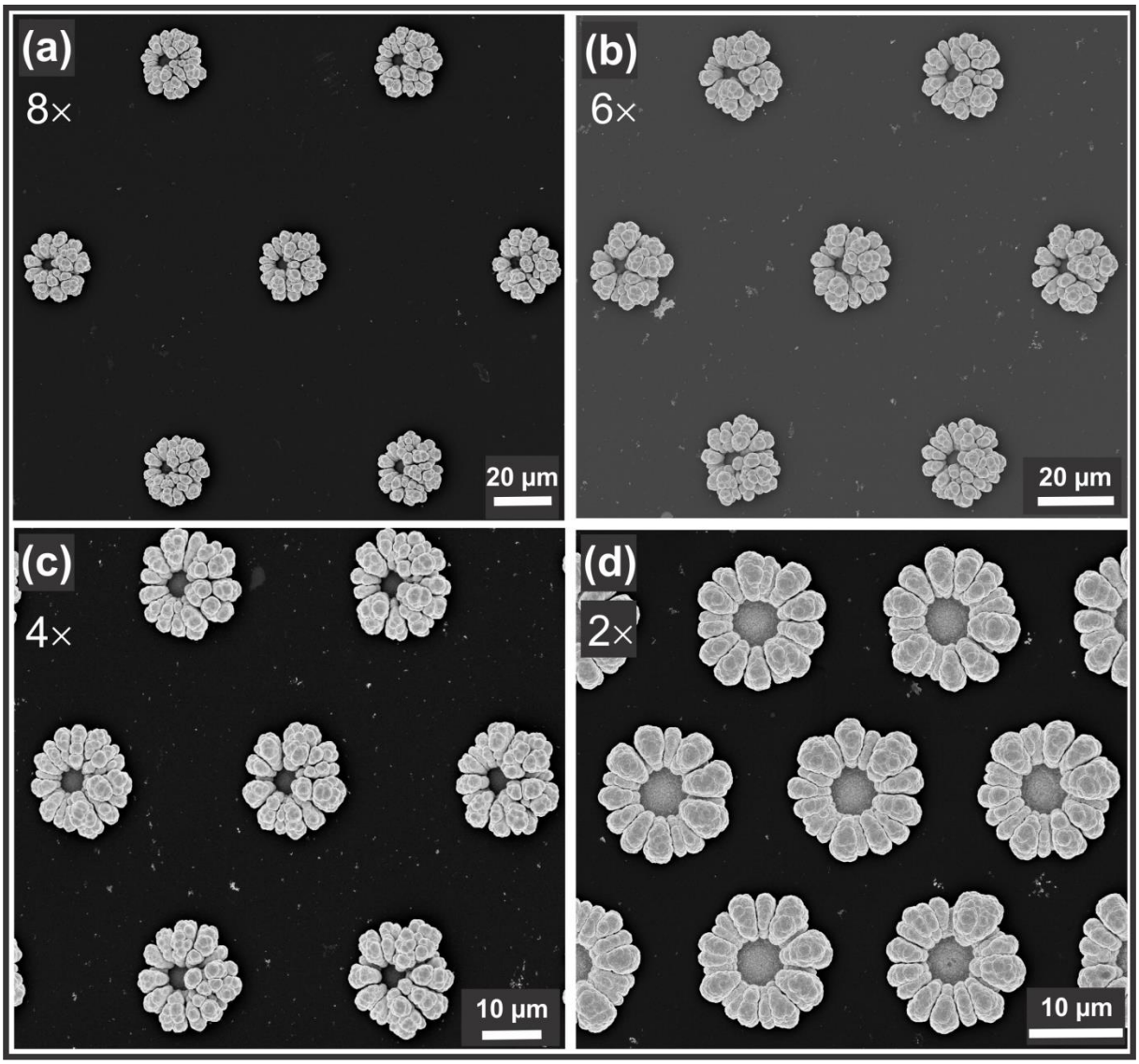

Figure 5: Scanning electron microscopy (SEM) images of 3D Pt structures deposited on Au MATFEs (91 microelectrodes, diameter 10 µm, depth 3.3 µm) having spacing: (a) 8×, (b) 6×, (c) 4×, and (d) 2× the diameter.

The diameters of the microstructures were determined by manually measuring the widest point of the deposit using the image-processing software Image J; the results are summarised in Table 1. The data shows a clear decrease in the average diameter of the deposits with decreasing centre-to-centre separation. As previously stated, this is likely due to more prevalent linear diffusion for MATFEs with smaller separations, causing less

outward growth of the microstructures at the surface once the µ-hole is filled.[20, 21] Smaller centre-to-centre separation also results in deposits with relatively larger diameters at the perimeter of the array compared to the rest of the array. This is because reducing the separation results in more significant linear-type diffusion pattern such as that experienced at a macrodisk electrode. Thus, the modified MATFEs will experience only partial radial diffusion at the edge of the array similar to a macrodisk electrode (represented in Figure 1, upper). Therefore, radial diffusion at the perimeter will cause greater outward growth of the microstructures in these locations compared with the more central microstructures in the array. This is also confirmed by measuring the height of the deposits on the outer edge which are fairly consistent for all separations (11.9 – 12.8 µm, Table 2), compared to the height of the inner deposits, which vary quite widely with electrode separation (5.1 – 11.6 µm).

Table 1: Parameters obtained for MATFEs with different centre-to-centre spacings: charge for deposition (Q), diameter of deposits, charge for desorbed hydrogen (Q_H), and electroactive surface area (ESA) calculated from the integration of H_2 desorption peak obtained in N_2-saturated 0.5 M H_2SO_4. Error bars represent one standard deviation over 91 electrodes for three repeat depositions (i.e. n = 273 for "all deposits").

Electrode spacing	Q for deposition / mC	Diameter of all deposits / µm	Diameter of inner deposits[1] / µm	Diameter of outer deposits[2] / µm	$Q_H = \int I\,dt$ / C	ESA / m^2
8×	11.13	23.8 ± 1.5	24.5 ± 0.9	23.1 ± 2.0	10.5×10^{-06}	4.98×10^{-06}
6×	7.56	21.5 ± 1.2	20.9 ± 0.8	22.0 ± 1.6	7.11×10^{-06}	3.39×10^{-06}
4×	5.00	19.9 ± 1.5	19.2 ± 0.9	20.5 ± 2.1	4.47×10^{-06}	2.13×10^{-06}
2×	3.11	14.8 ± 1.4	13.7 ± 0.8	15.9 ± 1.9	1.82×10^{-06}	0.87×10^{-06}

[1] Inner deposits are the 61 microstructures located in the centre of the array.
[2] Outer deposits are the 30 microstructures located at the edge of the array.

Table 2: Measured heights (using AFM) above the SU-8 layer of the platinum 3-dimensional deposits as a function of different centre-to-centre spacings. The average height of the deposits in the centre of the array (Inner) are compared to the average height of the deposits in the outer perimeter (Outer) of the array, where the deposits appear larger.

	Height of deposits / µm	
	Inner[1]	Outer[2]
8x	11.6 (± 0.9)	12.8 (± 0.9)
6x	10.3 (± 0.8)	12.5 (± 1.5)
4x	7.4 (± 0.9)	11.9 (± 0.9)
2x	5.1 (± 1.0)	11.9 (± 0.7)

[1] Inner deposits are the 61 microstructures located in the centre of the array.
[2] Outer deposits are the 30 microstructures located at the edge of the array.

3.2 Calculation of Electroactive Surface Area

The electroactive surface area (ESA) of the modified MATFEs was determined using the integrated charge under the hydrogen desorption peaks of cyclic voltammetry in 0.5 M H_2SO_4. Figure 6 shows the full potential scan of the electrodes in 0.5 M H_2SO_4, revealing the expected processes on platinum surfaces.[35, 36] The hydrogen desorption peaks occur between -0.23 V and 0.1 V. Assuming an atomic hydrogen monolayer coverage of 210 µC cm^{-2}, the ESA can be calculated using equation (4):[31, 37]

$$ESA = \frac{Q_H}{210\ \mu C\ \mathrm{cm}^{-2}} \quad (4)$$

where Q_H is the integrated area under the adsorption peaks. Table 1 shows the ESA values of the electrodeposited material as a function of electrode spacing. The surface area decreases systematically as the spacings decrease, with ca. 5.7 times smaller ESA for the 2× separation compared to the 8× separation. This is consistent with the much smaller sized deposits observed in the SEM images of the more closely spaced electrodes in Figure 5.

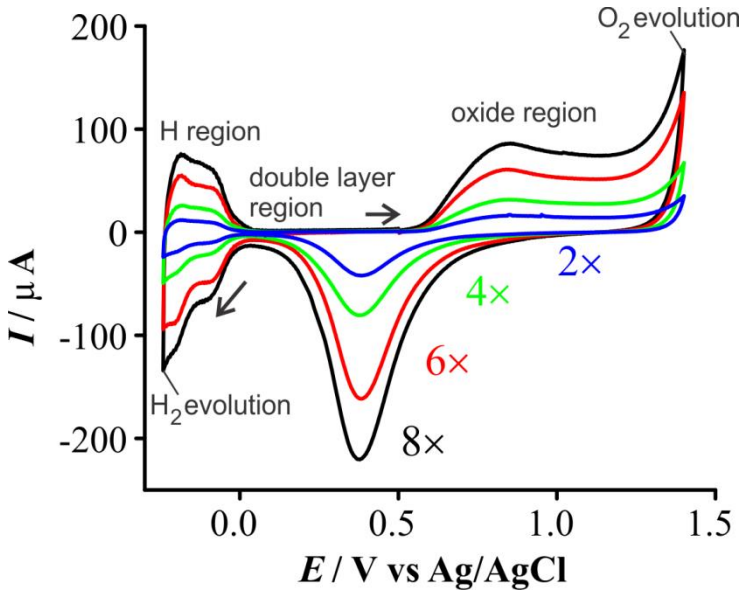

Figure 6: Cyclic voltammograms at 500 mVs^{-1} between +1.4 and −0.24 V recorded on the Pt-deposited Au MATFEs with different spacings in a N_2-saturated solution of 0.5 M H_2SO_4 vs stable Ag/AgCl reference electrode. The integrated area ($Q = I \times t$) of the H_2 desorption peaks (background subtracted) was used to calculate the electroactive surface area (ESA).

3.3 Electrode separation impact on modified microarray electrode performance for oxygen sensing

To study the effect on analytical responses, the modified electrodes were then utilised as sensing devices to detect a model analyte – oxygen gas – in a room temperature ionic liquid (RTIL). Oxygen is reduced in a one-electron process in dry aprotic RTILs, according to the following equation:[38, 39]

$$O_2 + e^- \rightleftharpoons O_2^{\bullet -} \quad (5)$$

Figure 7 shows linear sweep voltammetry (LSV) for the reduction of oxygen at different concentrations (1–30 % vol.) in the RTIL $[C_4mpyrr][NTf_2]$. The blank response in the absence of oxygen is shown as a dashed line. There is some non-Faradaic charging current and small impurities in the blank (common with ionic liquids), but generally the blank scan is featureless, so the reduction of oxygen can be easily observed and currents can be measured by background subtraction of the blank response. For the 8x separation (Figure 7a), the oxygen reduction voltammetry is more steady-state shaped, and becomes more peak-shaped as the separation decreases, suggesting more diffusional overlap and increased linear diffusion, as expected for more closely spaced electrodes. The same behaviour is also observed for a conventional redox probe, hexaammineruthenium (III) chloride ($[Ru(NH_3)_6]Cl_3$, in water (see Figure S2 in the supporting information).

For all four electrode separations, the current increases linearly with increasing concentration, and the calibration lines (shown as insets to the figures) are linear with $R^2 \geq 0.997$. The reduction peak potentials occur between ~-1.3 V and -1.9 V, and this difference can be explained by the use of the internal Au quasi-reference on the electrode device, which can experience some potential shifting. Since the peak currents (not potentials) are used in the calibration, the addition of an internal redox couple was not necessary, as the currents can be easily extracted from the voltammograms. Where the peak was not easily visible (e.g. for the 8× separation), a fixed potential was chosen to measure the currents, as shown in the dotted vertical line in Figure 7a, because the potential appeared to be mostly stable over the course of an experiment. The limit of detection (LOD) is relatively consistent over all the separations (between 1 and 2 % vol., see Table 3), and is similar to that reported in our previous work for oxygen sensing in RTILs on conventional (10× separation) MATFEs.[18]

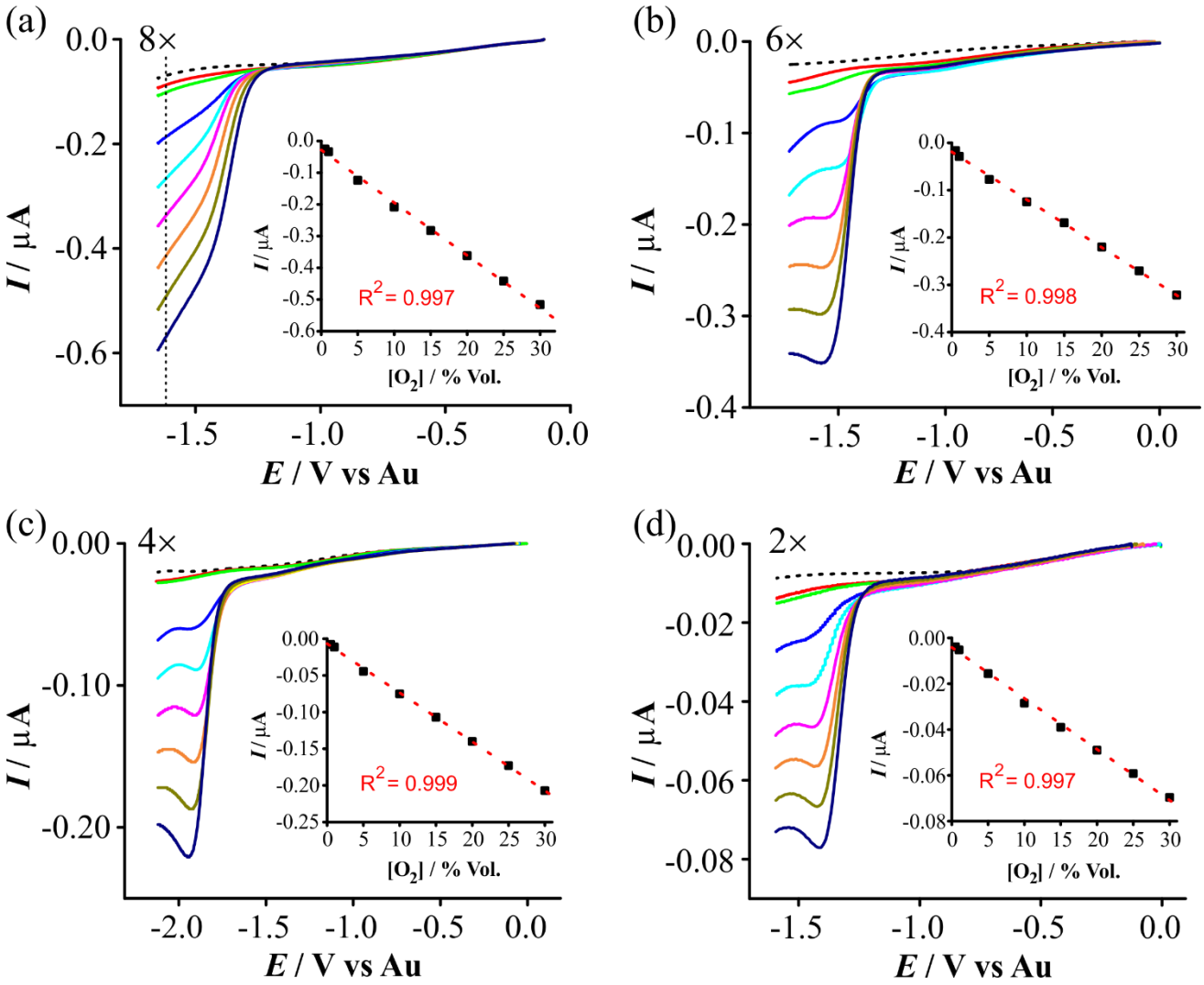

Figure 7: Linear sweep voltammetry (LSV) at 50 mVs^{-1} for different concentrations of oxygen ranging from 1 to 30 % vol. in [C_4mpyrr][NTf_2] recorded on the Pt modified Au MATFEs with different spacing (a) 8×, (b) 6×, (c) 4×, (d) 2×. The dashed voltammogram line shows the blank response in the absence of oxygen. The vertical dotted line in (a) shows the fixed potential at where the currents were extracted. For (b), (c), and (d) the currents were extracted from the peaks. The insets show the corresponding calibration plots with (background subtracted) currents vs [O_2] for different concentrations of oxygen gas.

Table 3: Analytical parameters including background-subtracted peak current (I_{O_2}/30 %), slope, limit of detection (LOD) and R^2 values for calibration line for oxygen reduction in [C_4mpyrr][NTf_2] on the Pt-deposited Au MATFEs with different centre-to-centre spacings: 8×, 6×, 4×, and 2× the diameter.

Electrode spacing	I_{O_2} @ 30 % / A	Slope / A%$^{-1}$	LOD / % O_2	R^2
8×	-5.1×10^{-7}	-1.70×10^{-8}	1.8	0.997
6×	-3.2×10^{-7}	-1.01×10^{-8}	1.5	0.998
4×	-2.1×10^{-7}	-0.67×10^{-8}	1.0	0.999
2×	-0.7×10^{-7}	-0.23×10^{-8}	1.9	0.997

Table 3 shows the current for 30 % vol. O_2, and the slope (sensitivity) of the calibration line of best fit for all four electrode separations. The current and sensitivity (slope) decrease as the spacing reduces, as expected from the smaller electroactive surface area (ESA) of the Pt deposits at smaller separations; Figure 8a shows this effect visually, with the calibration plots of peak current vs concentration plotted on the same graph. Figure 8b shows the same plot, but using current density (*J*), which was calculated by dividing the current (*I*) by the ESA (shown in Table 1). By dividing by the ESA, the current becomes independent of the electrode surface area, so current density is related to the rate of mass transfer. The sensitivity for the current density plot is almost the same for the different spacings, with slightly lower sensitivity observed in the most closely separated arrays (2×). This is expected, because although the deposits are the smallest, there are much smaller spacings between the electrodes and therefore slightly more overlapped diffusion during the oxygen sensing process compared to the more closely spaced electrodes.

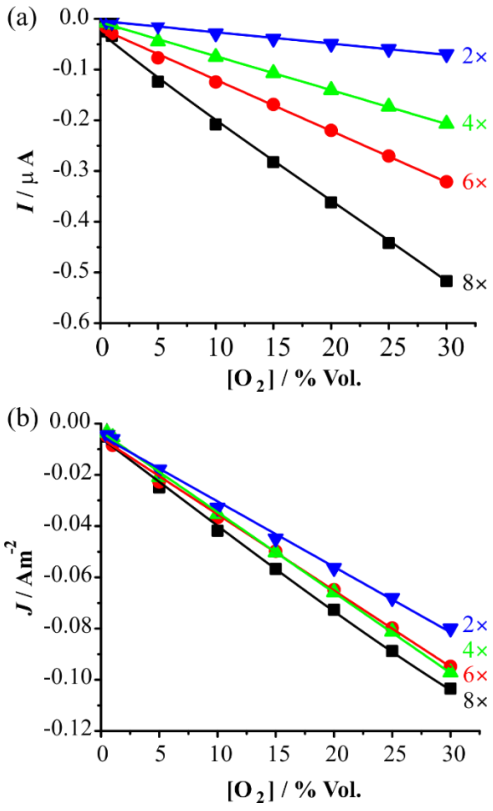

Figure 8: Plot of (a) absolute current (*I*) vs oxygen concentration and (b) current density (*J*) vs oxygen concentration, for the reduction of 1–30 % vol. oxygen in [C_4mpyrr][NTf_2] recorded on the Pt-deposited Au MATFEs with different centre-to-centre spacing: 8×, 6×, 4×, and 2×.

The diffusion layer thickness for inlaid electrodes can be estimated using the following expression: [40]

$$d = \sqrt{\pi D t} \quad (6)$$

Where *d* is the diffusion layer thickness, *D* is the diffusion coefficient of the analyte (5.49×10^{-10} m^2s^{-1} for O_2 in [C_4mpyrr][NTf_2] at 298 K),[41] and *t* is the time taken for the diffusion layer to evolve. From the onset of the O_2 reduction wave to the end of the linear sweep voltammogram is ca. 0.2 V, which corresponds to a time of 4 s at a scan rate of 50 mVs^{-1}. Hence by applying equation 6, the diffusion layer thickness in a typical scan is estimated to be ca. 83 µm. This is well above the nearest distance between neighbouring electrodes for all microarrays with different spacings (see Figure 5), showing that diffusion overlap is highly likely for these sensing experiments.

The microarrays utilised during these experiments only occupy a portion of the available space of the working electrode. In descending order, the microarrays occupy a WE area equivalent to ca. 64%, 36%, 16% and 4% of the full 1 mm WE. It is therefore important to consider the possibility of manufacturing MATFEs with the electrodes fully occupying the space available at the 1mm diameter WE to increase the overall current. A fully occupied WE would theoretically contain 142 µ-holes for the 8× separation, 252 µ-holes for the 6× separation, 567 µ-holes for the 4× separation and 2268 µ-holes for the 2× separation. The 2× array can therefore fit ca. 16 times the number of electrodes within the same electrode area as the 8× array. Assuming the currents are roughly additive as the number of electrodes in the array is increased, the 2× separation can give more than double the current (sensitivity) compared to the 8× separation – while the current density for the 2× separation is only ca. 20% lower vs that of the 8× separation (Figure 8). Therefore, careful consideration of the overall geometry and electrode spacing is needed when optimising the design of microelectrode arrays. Ultimately, the manufacturing limits will determine the maximum number of electrodes that are possible within the array.

While oxygen was used as a model analyte in this work, these arrays could also be used for a range of other electroanalytical applications, so long as careful attention is paid to both the analyte diffusion coefficient and the experimental timescale, to determine the most optimum electrode separation for the task.

4. Conclusions

The effect of microarray spacings on the deposition of Pt structures into microholes was investigated using MATFEs with different centre-to-centre separations. The spacing had a significant influence on the amount of Pt deposits when using the same plating bath and same deposition time. Surface areas of the deposits were found to decrease systematically as the spacing reduces, with 5.7 times the surface area for the 8× separation compared to the 2× separation. Larger structures were observed on the perimeter of array compared to the central electrodes, especially for the most closely spaced electrodes (2× separation), due to significant diffusion layer overlap with neighbouring electrodes in the array. The electrodes were used for oxygen detection in [C_4mpyrr][NTf_2], showing linear calibration graphs for all spacings. Sensitivity differences were observed due

to the different electroactive surface areas, however, current densities were comparable for all separations. The 2× separation can theoretically fit 16 times the number of electrodes in the same area compared to the 8× separation, which could increase the overall current responses and provide better analytical quantification. Reducing the spacing between electrodes could be especially useful for more viscous RTILs, or more slowly diffusing analytes. Here, diffusion layers will be even smaller, and electrodes can be closer together without giving significant diffusion overlap. This work suggests that careful consideration of the geometry should be undertaken when designing microelectrode arrays for electroanalytical applications.

Acknowledgments

DSS thanks the Australian Research Council for funding through a Future Fellowship [FT170100315]. The authors acknowledge the use of equipment of the Curtin University Electron Microscope Facility, which is partially funded by the University, State and Commonwealth Governments of Australia.

Table of Contents Figure

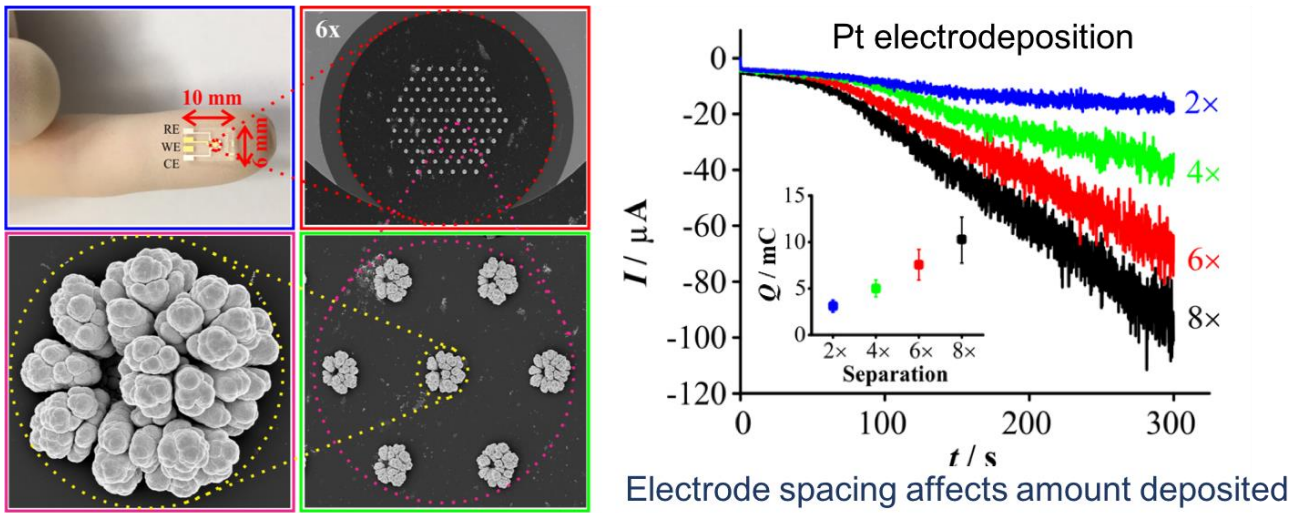

References

[1] M. Armand, F. Endres, D. MacFarlane, H. Ohno, B. Scrosati, ionic-liquid materials for the electrochemical challenges of the future, Nat. Mater., 8 (2009) 621-629.
[2] D.R. MacFarlane, M. Forsyth, P.R. Howlett, J.M. Pringle, J. Sun, G. Annat, W. Neil, E.I. Izgorodina, Ionic Liquids in Electrochemical Devices and Processes: Managing Interfacial Electrochemistry, Acc. Chem. Res., 40 (2007) 1165–1173.
[3] T. Kondo, I. Udagawa, T. Aikawa, H. Sakamoto, I. Shitanda, Y. Hosh, M. Itagaki, M. Yuasa, Enhanced Sensitivity for Electrochemical Detection Using Screen-Printed Diamond Electrodes via the Random Microelectrode Array Effect, Anal. Chem., 88 (2016) 1753–1759.
[4] J. Lee, G. Hussain, C.E. Banks, D.S. Silvester, Screen-Printed Graphite Electrodes as Low-Cost Devices for Oxygen Gas Detection in Room-Temperature Ionic Liquids, Sensors, 17 (2017) 1-13.
[5] J.P. Metters, R.O. Kadara, C.E. Banks, New directions in screen printed electroanalytical sensors: an overview of recent developments, Analyst, 136 (2011) 1067–1076.
[6] K. Murugappan, D.W.M. Arrigan, D.S. Silvester, Electrochemical Behavior of Chlorine on Platinum Microdisk and Screen-Printed Electrodes in a Room Temperature Ionic Liquid, J. Phys. Chem. C, 119 (2015) 23572-23579.
[7] K. Murugappan, D.S. Silvester, Sensors for Highly Toxic Gases: Methylamine and Hydrogen Chloride Detection at Low Concentrations in an Ionic Liquid on Pt Screen Printed Electrodes, Sensors, 15 (2015) 26866-26876.
[8] E.P. Randviir, D.A.C. Brownson, J.P. Metters, R.O. Kadara, C.E. Banks, The fabrication, characterisation and electrochemical investigation of screen-printed graphene electrodes, Phys. Chem. Chem. Phys., 16 (2014) 4598-4611.
[9] J. Lee, G. Du Plessis, D.W.M. Arrigan, D.S. Silvester, Towards improving the robustness of electrochemical gas sensors: impact of PMMA addition on the sensing of oxygen in an ionic liquid, Anal. Methods, 7 (2015) 7327-7335.
[10] J. Lee, D.S. Silvester, Electrochemical Detection of Explosive Compounds in an Ionic Liquid in Mixed Environments: Influence of Oxygen, Moisture, and Other Nitroaromatics on the Sensing Response, Australian Journal of Chemistry, 72 (2019) 122-129.
[11] H.A. Yu, J. Lee, S.W. Lewis, D.S. Silvester, Detection of 2,4,6-Trinitrotoluene Using a Miniaturized, Disposable Electrochemical Sensor with an Ionic Liquid Gel-Polymer Electrolyte Film, Anal. Chem., 89 (2017) 4729-4736.
[12] S. Hannah, M. Al-Hatmi, L. Gray, D.K. Corrigan, Low-cost, thin-film, mass-manufacturable carbon electrodes for detection of the neurotransmitter dopamine, Bioelectrochem., 133 (2020) 107480.
[13] J. Lee, G. Hussain, N. López-Salas, D.R. MacFarlane, D.S. Silvester, Thin films of poly(vinylidene fluoride-cohexafluoropropylene)-ionic liquid mixtures as amperometric gas sensing materials for oxygen and ammonia, Analyst, 145 (2020) 1915–1924.
[14] S. Doblinger, J. Lee, Z. Gurnah, D.S. Silvester, Detection of sulfur dioxide at low parts-per-million concentrations using low-cost planar electrodes with ionic liquid electrolytes, Anal. Chim. Acta, 1124 (2020) 156–165.
[15] E. Saygili, B. Orakci, M. Koprulu, A. Demirhan, E. Ilhan-Ayisigi, Y. Kilic, O. Yesil-Celiktas, Quantitative determination of H2O2 for detection of alanine aminotransferase using thin film electrodes, Anal. Biochem., 591 (2020) 113538.
[16] M.A. Eshan, M. Abdul Aziz, A. Rehman, A.S. Hakeem, M.A.A. Qasem, S.H.A. Ahmad, Aerosol-Assisted Chemical Vapor Deposition of Silver Thin Film Electrodes for Electrochemical Detection of 2-Nitrophenol, J. Electrochem. Soc., 165 (2018) B302.
[17] S.D. Branch, A.M. Lines, J. Lynch, J.M. Bello, W.R. Heineman, S.A. Bryan, Optically Transparent Thin-Film Electrode Chip for Spectroelectrochemical Sensing, Anal. Chem., 89 (2017) 7324–7332.
[18] J. Lee, D.S. Silvester, Low-cost microarray thin-film electrodes with ionic liquid gel-polymer electrolytes for miniaturised oxygen sensing, Analyst, 141 (2016) 3705-3713.
[19] G. Hussain, D.S. Silvester, Comparison of Voltammetric Techniques for Ammonia Sensing in Ionic Liquids, Electroanalysis (2018).
[20] G. Hussain, A.P. O'Mullane, D.S. Silvester, Modification of microelectrode with high surface area dendritic platinum 3D structures: enhanced sensitivity for oxygen detection in ionic liquids, Nanomaterials, 8 (2018) 735-748.
[21] G. Hussain, L. Aldous, D.S. Silvester, Preparation of platinum-based 'cauliflower microarrays' for enhanced ammonia gas sensing, Anal. Chim. Acta, 1048 (2019) 12-21.

[22] X. Huang, A.M. O'Mahony, R.G. Compton, Microelectrode arrays for electrochemistry: approaches to fabrication, Small, 5 (2009) 776-788.
[23] T.J. Davies, R.G. Compton, The cyclic and linear sweep voltammetry of regular and random arrays of microdisc electrodes: Theory, J. Electroanal. Chem., 585 (2005) 63–82.
[24] T.J. Davies, S. Ward-Jones, C.E. Banks, J. del Campo, R. Mas, F.X. Munoz, R.G. Compton, The cyclic and linear sweep voltammetry of regular arrays of microdisc electrodes: Fitting of experimental data, J. Electroanal. Chem., 585 (2005) 51–62.
[25] J. Guo, E. Lindner, Cyclic Voltammograms at Coplanar and Shallow Recessed Microdisk Electrode Arrays: Guidelines for Design and Experiment, Anal. Chem., 81 (2009) 130–136.
[26] S.J. Hood, D.K. Kampouris, R.O. Kadara, N. Jenkinson, F.J. del Campo, F.X. Munoz, C.E. Banks, Why 'the bigger the better' is not always the case when utilising microelectrode arrays: high density vs. low density arrays for the electroanalytical sensing of chromium(VI), Analyst, 134 (2009) 2301–2305.
[27] P. Tomčík, Microelectrode Arrays with Overlapped Diffusion Layers as Electroanalytical Detectors: Theory and Basic Applications, Sensors, 13 (2013) 13659-13684.
[28] Y. Saito, A Theoretical Study on the Diffusion Current at the Stationary Electrodes of Circular and Narrow Band Types, Rev. Polarogr., 15 (1968) 177–187.
[29] L.C.R. Alfred, K.B. Oldham, The steady state at a pair of hemispherical microelectrodes, J. Electroanal. Chem., 396 (1995) 257–263.
[30] S. Fletcher, M.D. Horne, Random assemblies of microelectrodes (RAM™ electrodes) for electrochemical studies, Electrochem. Commun., 1 (1999) 502-512.
[31] J.J. Burk, S.K. Buratto, Electrodeposition of Pt Nanoparticle Catalysts from H2Pt(OH)6 and Their Application in PEM Fuel Cells., J. Phys. Chem., 117 (2013) 18957-18966.
[32] M.N. Desic, M.M. Popovic, M.D. Obradovic, L.M. Vracar, B.M. Grgur, Study of gold-platinum and platinum-gold surface modification and its influence on hydrogen evolution and oxygen reduction, J. Serb. Chem. Soc., 70 (2005) 231-242.
[33] R.G. Compton, C.E. Banks, Understanding voltammetry, World Scientific Publishing Co., Singapore, 2007.
[34] T.J. Davies, C.E. Banks, R.G. Compton, Voltammetry at spatially heterogeneous electrodes, J Solid State Electrochem, 9 (2005) 797–808.
[35] V. Climent, J.M. Feliu, Thirty years of platinum single crystal electrochemistry., J. Solid State Electrochem., 15 (2011) 1297–1315.
[36] L. Jacobse, S.J. Raaijman, M.T.M. Koper, The reactivity of platinum microelectrodes., Phys. Chem. Chem. Phys., 18 (2016) 28451–28457.
[37] M. Lukaszewski, M. Soszko, A. Czerwinski, Electrochemical methods of real surface area determination of noble metal electrodes – an overview, Int. J. Electrochem. Sci., 11 (2016) 4442-4469.
[38] M.C. Buzzeo, O.V. Klymenko, J.D. Wadhawan, C. Hardacre, R.G. Compton, Voltammetry of Oxygen in the Room-Temperature Ionic Liquids 1-Ethyl-3-methylimidazolium Bis((trifluoromethyl)sulfonyl)imide and Hexyltriethylammonium Bis((trifluoromethyl)sulfonyl)imide: One-Electron Reduction To Form Superoxide. Steady-State and Transient Behavior in the Same Cyclic Voltammogram Resulting from Widely Different Diffusion Coefficients of Oxygen and Superoxide, J. Phys. Chem. A, 107 (2003) 8872-8878.
[39] A. Khan, C.A. Gunawan, C. Zhao, Oxygen Reduction Reaction in Ionic Liquids: Fundamentals and Applications in Energy and Sensors, ACS Sustainable Chem. Eng., 5 (2017) 3698-3715.
[40] A. Molina, J. González, E. Labordaab, R.G. Compton, On the meaning of the diffusion layer thickness for slow electrode reactions, Phys. Chem. Chem. Phys., 15 (2013) 2381-2388.
[41] X.-J. Huang, E.I. Rogers, C. Hardacre, R.G. Compton, The Reduction of Oxygen in Various Room Temperature Ionic Liquids in the Temperature Range 293-318 K: Exploring the Applicability of the Stokes-Einstein Relationship in Room Temperature Ionic Liquids, J. Phys. Chem. B, 113 (2009) 8953–8959.